Supplement of Biogeosciences, 22, 7709–7724, 2025
https://doi.org/10.5194/bg-22-7709-2025-supplement

Biogeosciences Open Access EGU

Supplement of

Assessing the impact of riverine water on the Northwest Pacific using normalized Total Alkalinity

Tatsuki Tokoro et al.

Correspondence to: Tatsuki Tokoro (tokoro.tatsuki@nies.go.jp)

S1. Vertical profile and advection of nTA and nDIC.

The vertical profiles of nTA and nDIC were calculated using the vertical distribution data of SSS, TA, and DIC in the GLODAP. First, the GLODAP data was re-grided to 1°×1° and 0.1 year as for the surface data. The vertical direction was re-grided according to the JCOPE2 depth scale (depth -5 m, -10 m, and every -10 m thereafter), which was used to calculate the MLD. In this study, nTA and nDIC were calculated up to a depth of 150 m. Vertical profiles in Areas A and B were finally produced by horizontally averaging the gridded data for each area. Because the data regression used for the surface data could not be applied to the profile data, the temporal resolution of the profiles was insufficient to calculate the vertical advection. Therefore, annual variations were calculated from the average over 20 years and these annual variations were assumed to be repeated 20 times.

The nDIC in July in Equation 5 was determined using the average of the data corresponding to 0.6 years because the temporal resolution of the processed data was 0.1 year (Figure S1). No significant trend in the vertical gradient in July for nTA could be identified for either Areas A or B. Notably, nTA in Area A was significantly higher than that in Area B because of the higher salinity in Area B, which was lower than the MLD (approximately 10 m depth in July) compared to Area A. This was not due to riverine water, but because Area B was located at the northern limit of the North Pacific Tropical Water, which is a subsurface water mass that originally formed at the sea surface at 20–30°N in the North Pacific with strong evaporation. In contrast, the nDIC gradients were significant; they ranged from (-0.72 ± 0.20) × depth + (1974.86 ± 18.01) μmol kg^{-1} m^{-1} in Area A to (-0.30 ± 0.04) × depth + (1966.54 ± 3.20) μmol kg^{-1} m^{-1} in Area B. These results indicated that the changes in TA owing to vertical advection were not sufficiently large to cause significant effects. Vertical advection is expected to increase the nDIC. The effect should result in an increase in *dAB* of nDIC because of the larger slope in Area A than in Area B.

As the nDIC profile in July and other time steps still contained missing values, the following process was applied: 1) The nDIC profile in July (nDIC (*July, MLD*) in Equation 5) was determined from the linear approximations described above. 2) The nDIC at the mixed layer (nDIC(*t, MLD*) in Equation 5) was calculated as the average from the surface (depth = -5 m) to a depth of the JCOPE2 scale, which is the nearest neighborhood of the MLD at that timestep (Figure S2), under the assumption that nDIC within the mixed layer was well mixed and uniform in depth (Figure S2). Missing nDIC between 0.6 and 0.9 years were substituted for linear interpolations of pre- and post-

non-missing values. The standard deviation of the nDIC within the mixed layer in step 2) and the propagation of the error in the approximate line in step 1) were used to calculate the error in the vertical advection term.

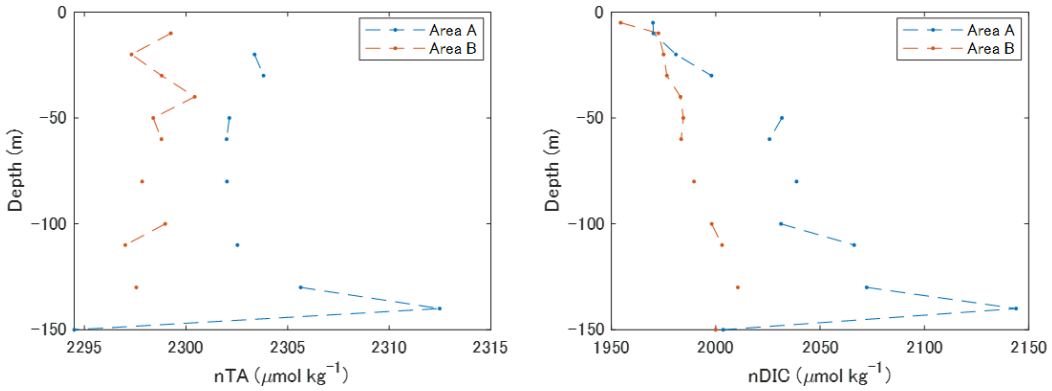

Figure S1. Vertical profiles of nTA and nDIC in July

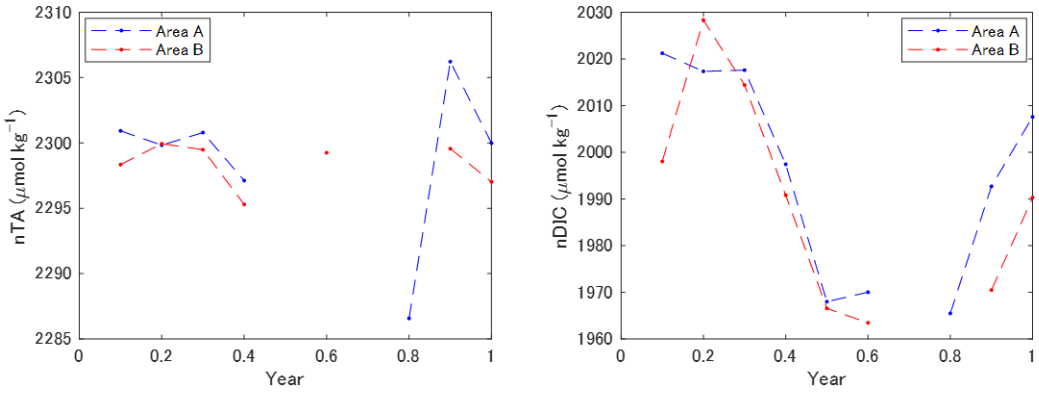

Figure S2. Seasonal nTA and nDIC at the mixed layer depth

S2. Riverine water supply from mainland of Japan.

The following 37 rivers on the Pacific coast adjacent to Area A were selected as riverine water sources. The flows of each river for the years 2000-2019 were obtained from the Water Information System database of the Ministry of Land, Infrastructure, Transport, and Tourism of Japan (http://www1.river.go.jp/). However, because this database contains many missing values, the total flow rates of riverine water were calculated using the following procedures: 1): The annual missing data for each river were replaced with the average value of that river over the period of 2000-2019. Then, the total annual flow rate of riverine water was calculated as the sum of all rivers. 2):

The top five rivers with the largest flow rate (9% of all rivers) were selected to represent seasonal variability of the total flow rate. For each river, single year with the median flow rate and complete monthly data was selected (Tone River in 2002, Tenryū River in 2009, Kiso River in 2009, Yodo River in 2000, and Shimanto River in 2008). The monthly flow rates from these representative years were first averaged across the five rivers for each calendar month to obtain a composite monthly flow pattern. The annual mean flow rate was then calculated as the sum of these twelve-monthly averages. Finally, the fraction of each month was defined as the ratio of the monthly flow rate to the annual one. 3): The faction was assumed to be representative seasonal distribution applied to the entire study period (2000-2019), and the overall data was obtained by multiplying the annual totals of the 37 rivers by the monthly fractions (Figure S3).

Selected Rivers: Tone River, Arakawa River, Tama River, Tsurumi River, Fuji River, Kano River, Abe River, Ōi River, Kiku River, Tenryū River, Toyo River, Yahagi River, Shōnai River, Kiso River, Suzuka River, Kumozu River, Kushida River, Miya River, Kumano River, Yamato River, Yodo River, Ibo River, Saba River, Ōta River, Ahida River, Takahashi River, Asahi River, Yoshii River, Oze River, Shigenobu River, Hiji River, Shimanto River, Niyodo River, Monobe River, Naka River, Yoshino River

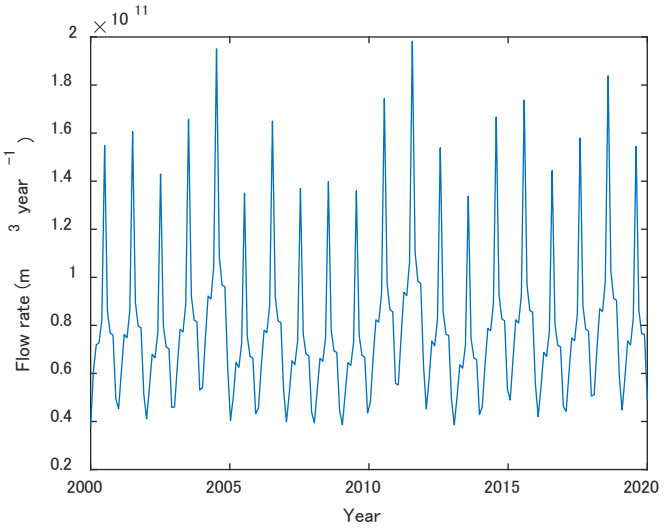

Figure S3. Flow rate of riverine water to Area A

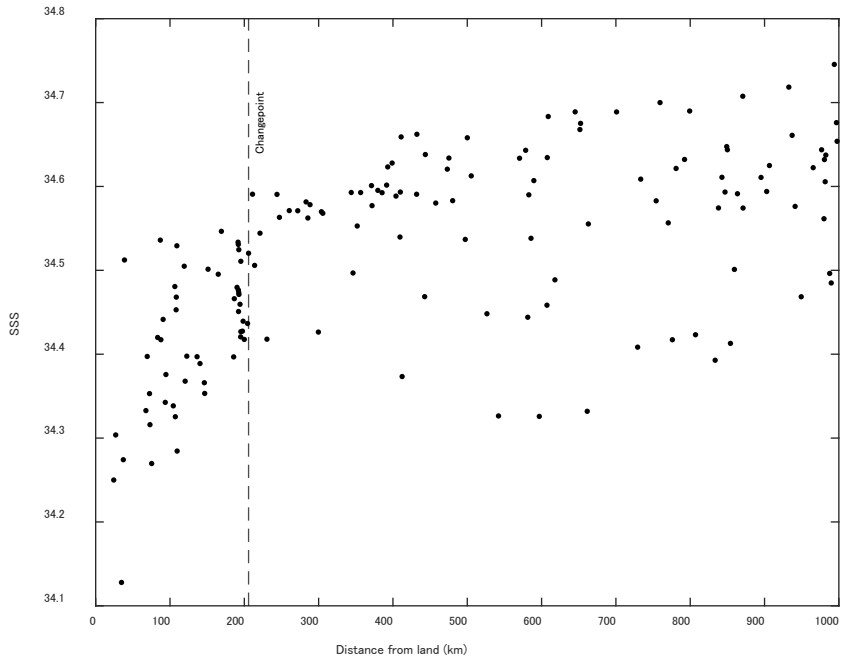

Figure S4. Scatterplot showing the distance from the mainland of Japan and SSS (south of 37°N).

The dotted line (210 km) indicates the distance where the mean SSS south of 37°N changed abruptly, as determined using change-point analysis.

Table S1. Average and standard deviation of re-gridding and Fourier regressed data for the entire study area. Values in the bottom row of brackets in each cell are from the previous study (Tokoro et al., 2023).

Parameter (Unit)	Re-gridded data n = 48289	Fourier regressed data n = 65200
SST (C°)	21.59 ± 5.63 (21.63 ± 5.66)	22.08 ± 5.11 (22.29 ± 5.06)
SSS (-)	34.50 ± 0.38 (34.51 ± 0.37)	34.52 ± 0.34 (34.54 ± 0.33)
fCO_{2water} (µatm)	348.39 ± 30.91 (348.56 ± 30.94)	347.54 ± 31.87 (348.21 ± 31.88)
fCO_{2air} (µatm)	384.95 ± 12.76 (385.79 ± 11.91)	383.95 ± 13.92 (383.65 ± 13.87)
TA (µmol kg^{-1})	2272.92 ± 15.83 (2272.99 ± 15.76)	2272.17 ± 14.92 (2272.15 ± 14.92)
DIC (µmol kg^{-1})	1965.32 ± 44.16 (1965.91 ± 44.59)	1960.29 ± 37.04 (1959.68 ± 36.82)

Table S2. Average and standard deviation of relevant parameters in Areas A and B. The values in brackets within the TA and DIC columns indicate the respective values of nTA and nDIC.

Parameter (Unit)	Area A n = 231800	Area B n = 233200
SST (C°)	22.02 ± 3.77	22.86 ± 3.64
SSS (-)	34.41 ± 0.29	34.58 ± 0.22
fCO_{2water} (µatm)	341.11 ± 24.11	344.76 ± 29.78
TA (µmol kg^{-1})	2264.42 ± 14.53 (2303.59 ± 5.51)	2271.69 ± 12.30 (2299.31 ± 3.76)
DIC (µmol kg^{-1})	1916.41 ± 31.95 (1985.32 ± 23.65)	1951.32 ± 25.04 (1974.99 ± 17.95)

Table S3. Contributions of each explanatory variable on *dAB* of seawater fCO_2, pH, and Ω_{arg}. The values in the upper row are the averages in the PLS analysis. Those in the lower rows show the results of the equilibrium calculations using the values of Area B and the respective *dAB* values.

Explanatory Variable	Seawater CO_2 (µatm)	pH (-)	Ω_{arg} (-)
SST	-12.01	+0.01	-0.02
(C°)	-11.73	+0.01	-0.02
SSS	-2.22	+0.00	-0.01
(-)	-1.60	+0.00	+0.01
nTA	-6.29	+0.01	+0.04
(µmol kg^{-1})	-5.43	+0.01	+0.05
nDIC	+16.90	-0.02	-0.10
(µmol kg^{-1})	+17.11	-0.02	-0.11

References

Tokoro, T., Nakaoka, S., Takao, S., Saito, S., Sasano, D., Enyo, K., Ishii, M., Kosugi, N., and Nojiri, Y.: Statistical analysis of spatiotemporal variations of air-sea CO_2 fluxes in the Kuroshio region, JGR Oceans, 128. https://doi.org/10.1029/2023JC019762, 2023.